THE JOURNAL OF PHYSICAL CHEMISTRY B

Article

pubs.acs.org/JPCB

Increasing ^{13}C CP-MAS NMR Resolution Using Single Crystals: Application to Model Octaethyl Porphyrins

Sneha Dugar,[†,‡] Riqiang Fu,*[,‡] and Naresh S. Dalal*[,†,‡]

[†]Department of Chemistry and Biochemistry, Florida State University, Tallahassee, Florida 32306, United States

[‡]National High Magnetic Field Laboratory, Florida State University, 1800 E. Paul Dirac Drive, Tallahassee, Florida 32310, United States

Supporting Information

ABSTRACT: Octaethyl porphyrin (OEP) and its Ni and Zn derivatives are considered as model compounds in biochemical, photophysical, and fossil fuel chemistry. They have thus been investigated by high-resolution solid-state ^{13}C NMR using powders, but peak assignment has been difficult because of large line widths. Arguing that a significant cause of broadening might be the anisotropic bulk magnetic susceptibility, we utilized single crystals in our ^{13}C cross-polarization magic angle spinning (CP-MAS) measurements and observed a nearly 2-fold line narrowing. This enhanced resolution enabled us to assign chemical shifts to each carbon for all the three compounds. The new assignments are now in agreement with X-ray structural data and allowed us to probe the motional dynamics of the methyl and methylene carbons of the OEP side chains. It is apparent that the use of single crystals in ^{13}C CP-MAS measurements has a significantly wider impact than previously thought.

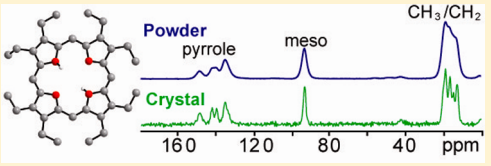

1. INTRODUCTION

Porphyrins and metalloporphyrins have been extensively studied because of their wide significance in biological and all photochemical and photophysical processes[1,2] as well as in fossil fuel chemistry.[3] Octaethyl porphyrins (OEP) with their symmetry and close relation to the native porphyrins, such as those with Zn and Ni, are considered as good models.[1,2] In OEP, eight ethyl groups are linked to the beta carbon (C_β) atoms of the pyrrole ring and two hydrogens are attached to two opposite pairs of nitrogens on the inner part of the porphyrin skeletal (Figure 1). One important issue has thus been whether OEP has two N−H tautomers or just one. Variable-temperature NMR studies on OEP in solution have shown that the tautomeric process is dynamic since only one set of signals was observed in fluid solutions, but peak splitting was noted in frozen samples, implying that the tautomeric dynamics is fast on the NMR time scale (millisecond) at room temperature but slow in frozen solutions.[4−6] To examine this question in the solid phase, pioneering NMR studies were carried out by Okazaki and McDowell,[7] and by Frydman et al.,[8] using the then newly developed high-resolution solid-state NMR technique of cross polarization,[9] combined with magic angle sample spinning (CP-MAS).[10−12] Okazaki and McDowell were able to resolve some of the ^{13}C peaks for OEP, but did not find evidence of splitting due to tautomerism. The assignments of the peaks in the ethyl region were also ambiguous, because of severe peak overlapping. On the other hand, Frydman et al.[8] carried out what appears to be a difficult task, the temperature dependence of CP-MAS on OEP,[8] and showed evidence of tautomerism. However, despite significantly new information, it was not possible to assign all the peaks to their respective carbons, especially in the ethyl side-chain region, because of peak broadening and overlapping.[7,8]

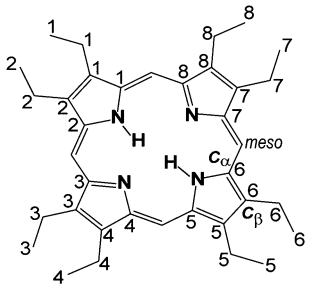

Figure 1. Structure of OEP showing the labeling scheme used in the following figures.

We envisaged that a significant cause of broadening might be that due to anisotropic bulk magnetic susceptibility (ABMS), as has been discussed in detail in 1981 by Garroway and co-workers.[13] These authors also emphasized that ABMS broadening could be obviated by use of a single crystal instead of powder in MAS measurements. They estimated that for ^{13}C NMR of most organic materials the reduction might be 20−30%, and the general impression seems to have been that it is not worthwhile growing crystals, even when easy to grow. In 1997, however, MAS studies using single crystals of squaric acid, $H_2C_4O_4$, a model hydrogen-bonded ferroelectric material, reported a significantly larger effect, enabling much deeper

Received: March 6, 2012
Revised: June 7, 2012
Published: June 8, 2012

understanding of hydrogen-bonding and its cooperative effects in ferroelectric materials.[14] Vasa et al.[15,16] and Kunath-Fandrei et.al.[17] also showed a better resolution on using a single crystal for MAS rather than powder. With the view of further exploration along this line, and also shedding more light on the molecular structures of solid porphyrins, we initiated CP-MAS studies on OEP and its Ni and Zn analogues, henceforth NiOEP and ZnOEP, respectively. We observed nearly 2-fold narrower peaks compared to the use of powders for all three compounds. This enhanced resolution enabled us to assign ^{13}C signals of each carbon and resolve some of the ambiguities in their earlier assignments.[7,8] It also enabled us to study the temperature dependence of relaxation times (T_1) of individual ^{13}C sites of the methyl and methylene carbons in NiOEP, and characterize their motional parameters for the first time.

2. EXPERIMENTAL SECTION

Octaethyl porphyrin, OEP, ZnOEP, and NiOEP were all purchased from Sigma Aldrich. Their single crystals were grown by slow evaporation from carbon disulfide (CS_2) at room temperature (RT). The single crystals used in the various NMR measurements were fully characterized by single-crystal X-ray diffraction. The solved structures were in good agreement with earlier reported X-ray studies[18−20] on these. ^{13}C CP-MAS NMR spectra were obtained with a spinning frequency of 7 kHz on a Bruker DMX 300 NMR spectrometer, where the ^1H and ^{13}C Larmor frequencies are 300.13 and 75.46 MHz, respectively. ^{13}C signals were enhanced by CP from protons, which was achieved through the Hartmann−Hahn matching condition, and then detected while the protons were decoupled using the two-pulse phase modulation (TPPM) decoupling sequence.[21] During CP, the ^1H spin-lock field of 50.5 kHz was used with a contact time of 1 ms. Glycine (the carbonyl peak at 175.0 ppm) was used as an external chemical shift reference and for setting up the CP condition. Deconvolution was performed using OriginPro8.5.0SR1. The resolution enhancement for the crystal samples was calculated by using the line width at half-height of the meso carbon signals since these signals did not show any overlap.

Two NMR methods were used to aid the peak assignments. First, the dipolar dephasing experiments[22,23] were carried out to distinguish the methyl ($-CH_3$) and methylene ($-CH_2$) resonances. In dipolar dephasing, following CP, a delay (two rotor periods) is inserted before the ^{13}C acquisition. In the middle of this delay, a 180° ^{13}C pulse is applied to refocus the ^{13}C chemical shifts, while the ^1H decoupling is turned off for a certain time (i.e., dephasing time) to allow the dephase of the ^{13}C magnetization, depending on their dipolar interactions with nearby protons. The magnetization corresponding to strong $^1H-^{13}C$ dipolar couplings (e.g., methylene group) dephases fast while the signals from the nonprotonated and methyl carbons dephase rather slow. Second, ^{13}C $T_{1\rho}$ measurements were performed to identify signals from the C_α and C_β carbons. $T_{1\rho}$ measurements are used for characterization of slow dynamics. As can be seen from the porphyrin structure, the C_α and C_β are rigid nuclei and hence their motions are in the time scale of a few milliseconds. Due to the close proximity of the C_β atoms to the rapidly rotating methyl groups, its $T_{1\rho}$ is shorter than C_α. Hence by doing $T_{1\rho}$ measurements, one can distinguish between the two nuclei. After CP enhancement, the ^{13}C magnetization is spin-locked for a period of time, i.e., spin-lock time, followed by acquisition under proton decoupling. During the spin lock, the C_β, due to its proximity to the rotating side chains, would relax faster than C_α. By comparing the signal intensities at two different spin-lock times, we can distinguish the signals coming from the C_α and C_β atoms.

The spin−lattice relaxation time, T_1 for ^{13}C (enhanced by CP) was measured using the inversion recovery pulse sequence ($\pi-\tau-\pi/2$) and then fitting the signals to

$$M_z(\tau) = M_\infty[1 - 2\exp(-\tau/T_1)]$$

For inversion recovery, 16 delay periods were used ranging from 0.001 to 50 s with a recycle delay of 2 s. 2000 scans were acquired at each temperature. Sample temperature was controlled within ±0.1 K using a Bruker BVT-2000 unit. The single crystal was packed at the center of a MAS rotor flanked with a Teflon tape.

3. RESULTS AND DISCUSSION

Figure 1 shows an approximate two-dimensional structure of OEP with the labeling of ^{13}C atoms. The high-resolution solid-state ^{13}C spectra of powder and crystal OEP at RT are shown in Figure 2. Clearly, the use of a single crystal as compared to a

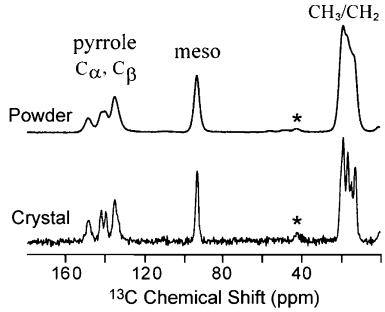

Figure 2. ^{13}C CP-MAS spectra of OEP in powder and single-crystal forms. The asterisk represents the spinning side bands. See text for peak assignment.

powder gave a near-2-fold enhancement. For example, the peak width at half-height for the meso carbons decreased from 2.8 to 1.6 pm resulting in a near-2-fold enhancement in resolution. This enhanced resolution enabled us to make a more definitive assignment of the chemical shifts.[7,8] The measured chemical shifts are collated in Table 1 with the C numbers in parentheses corresponding to Figure 1. Initial peak assignments were made based on ref 8. The ethyl region showed some spectral overlap, so we carried out the dipolar dephasing experiments to identify the CH_2 and CH_3 peaks.[22,23]

Figure 3A shows the spectra acquired after 2 μs dipolar dephasing time with signals from both CH_2 and CH_3 carbons while Figure 3B shows the spectra (with deconvolution of peaks) after a delay of 80 μs with signals only from the CH_3 carbons. Figure 3C shows the subtraction spectrum of (B) from (A) with signals only from the methylene carbons and its deconvolution. Deconvolution of these resonance peaks showed that there are four peaks each for CH_3 (20.2, 16.9, 16.3, 12.6 ppm) and CH_2 (19.2, 18.6, 14.7, 13.0 ppm) carbons and their relative intensities are almost the same.

The presence of the four signals of the CH_2 carbons can be rationalized by taking a close look at the crystal structure of OEP.[18] We do this by a "distance approach". When the molecules pack into a crystal, they form an orderly arrangement, due to crystal packing. As a result, the chemical shifts of

dx.doi.org/10.1021/jp302189r | J. Phys. Chem. B 2012, 116, 9215−9222

Table 1. ^{13}C Chemical Shifts (ppm) of CP-MAS NMR from Single Crystals OEP, NiOEP, and ZnOEP and Their Comparison with Powder Data[a]

	C_α	C_β	mesoC	CH_2	CH_3	ref
single-crystal H_2OEP	150.5[b] (3,7)	143.1[b] (3,7)	93.4	19.2 (3,7)	20.2 (2,6)	this work
	149.3[b] (4,8)	140.8[b] (4,8)		18.6 (4,8)	16.9 (3,7)	
	135.0[c] (1,2,5,6)	136.5[c] (1,2,5,6)		14.7 (1,5)	16.3 (4,8)	
				13.0 (2,6)	12.6 (1,5)	
powder H_2OEP	149.9[c]	142.3[c]	94.9	21.3	21.3	7
	137.0[b]	137.0[b]		18.1	18.1	
				14.0	14.0	
powder H_2OEP	149.9[b]	142.4[b]	95.0	19.4	18.0	8
	137.0[c]	137.0[c]		15.3	16.0	
					13.5	
single-crystal NiOEP	138.7	140.3	94.7	16.0 (2,4,6,8)	18.5	this work
				14.6 (1,3,5,7)		
powder NiOEP	140.4	140.4	95.9	20.1	20.1	7
crystal/powder ZnOEP	135.5 (1,5)	136.0 (1,2,5,6)	92.9	12.8 (1,5)	15.6 (4,8)	this work
	139.1 (2,6)	138.9 (3,4,7,8)		15.1 (2,6)	17.2 (1,5)	
	142.4 (3,4,7,8)			19.5 (3,4,7,8)	18.4 (2,3,6,7)	
powder ZnOEP	143.9	140.0	94.1	19.3	19.3	7
		136.4		17.3	17.3	

[a]The numbers in parentheses indicate the carbon atoms (Figure 1). [b]Indicates peaks appearing downfield (large chemical shift value) belonging to the −N═pyrrolenine-like ring. [c]Indicates peaks appearing upfield (less chemical shift value) belonging to the N−H pyrrole-like ring. Only relative positions should be compared and not the exact chemical shift values, because of the difference in the reference samples of this work and refs 7 and 8. TMS was used as external references in refs 7 and 8, while this work used glycine. Note that our assignments (relative positions) for some of the methyl and methylene carbons differ from those reported in refs 7 and 8.

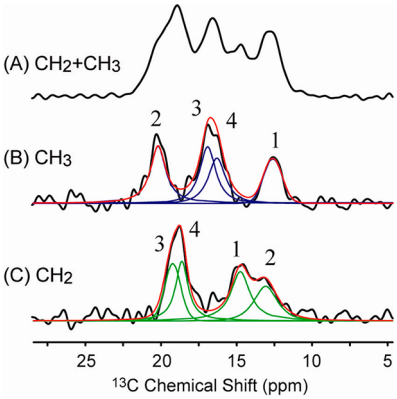

Figure 3. Dipolar-dephased ^{13}C CP-MAS spectra of a crystal for ethyl region of OEP (A) after a dephasing time of 2 μs showing both the CH_2 and the CH_3 peaks, (B) after a dephasing of 80 μs showing only the CH_3 peaks with the deconvoluted four peaks, and (C) subtraction of (B) from (A) showing only the CH_2 peaks with the four deconvoluted peaks. Atom labeling follows Figure 1.

the methylene carbons are affected not only by the π-electron cloud of its own ring but also by that of the neighboring porphyrin molecules. The former effect is the same on all CH_2 carbons, while the latter is strongly related to the distances of the methylene carbons to the porphyrin moieties of the neighboring molecule. Thus, the local chemical environment of the methylene carbon depends on its distance from the π-electron cloud of the neighboring molecule. From the crystal structure[18] (and Table SI-1, Supporting Information), it was seen that the methylene carbons are in four different environments. Since the influence of the neighboring π-electron cloud is different on different methylene carbons, the isotropic−chemical shift should also be different. This correlates with the observed 1:1:1:1 intensity ratio of the methylene carbons.

In order to differentiate between the local environments of the methylene carbons, we calculated the two shortest distances of the methylene carbon to the closest atoms on the neighboring porphyrin moiety using the crystal structure of OEP. Only the atoms of the core porphyrin (C_α, C_β, meso (C_m), and N atoms) were considered since they form the π-electron cloud.

We noticed that the four CH_2 carbons 1, 2, 3, and 4 (labeling shown in Figure 1) are at different distances to the closest atoms of the nearby porphyrin molecule (Table SI-1, Supporting Information). They should thus be in four different magnetically inequivalent environments and hence show four isotropic chemical shifts. This is indeed found to be the case. Figure 3C shows the individual peaks from four different CH_2 carbons. $CH_2(1)$ is at the shortest distance; it should be influenced greatly from the π-electron cloud of the neighboring molecule. But $CH_2(2)$ has more spatial proximity to the center of the π-electron cloud (N atoms), so it becomes most shielded and appears upfield at 13.0 ppm. Correspondingly, the peaks at 14.7, 18.6, and 19.2 ppm are assigned to $CH_2(1)$, -(4), and -(3), respectively. It is noted that $CH_2(5)$ has the same electronic environment as $CH_2(1)$, so they show only one peak. Similarly, CH_2 carbons (6), (7), and (8) are the same as (2), (3), and (4), respectively. This is also in conjunction with the fact that the crystal structure of OEP has $P\bar{1}$ symmetry.

Using the same distance approach (Table SI-1, Supporting Information), the CH_3 peaks at 12.6, 16.3, 16.9, and 20.2 ppm could be assigned to carbons (1), (4), (3), and (2), respectively. Methyl carbons (5), (6), (7), and (8) have the same electronic environment as (1), (2), (3), and (4). This also explains the observed 1:1:1:1 intensity ratio. It should be noted that the CH_3 and CH_2 peaks show a strong overlap. This can be attributed to the fact that they are strongly influenced by the π-electron cloud of the neighboring molecules. Figure 4 shows the ethyl region for OEP with the peaks from CH_3 and CH_2

dx.doi.org/10.1021/jp302189r | J. Phys. Chem. B 2012, 116, 9215−9222

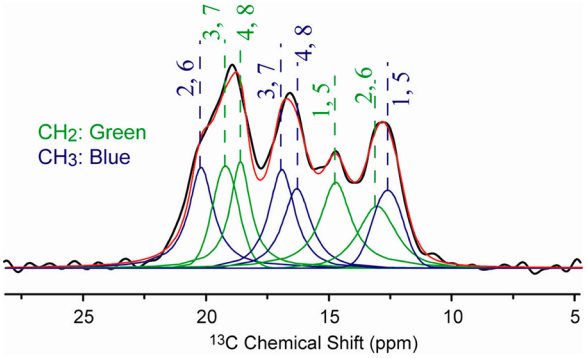

Figure 4. ^{13}C CP-MAS of crystal OEP in the ethyl region with the CH_2 and CH_3 peaks highlighted.

clearly identified. This peak distinction was possible *only* because of the near 2-fold enhancement in resolution by using single crystals.

To identify the resonance signals of the C_α and C_β carbons, we made the $T_{1\rho}$ measurements as described in the Experimental Section. Figure 5A shows the spectra of the

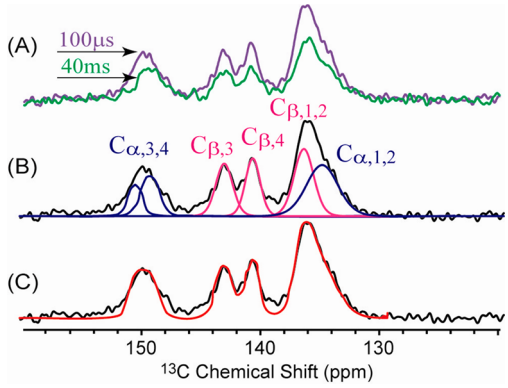

Figure 5. Peak assignment of the pyrrole region for crystal H_2OEP by $T_{1\rho}$ measurements using a spin-lock time of (A) 100 μs and 40 ms. (B) Deconvoluted spectra showing the α- and the β-carbons. (C) Red curve, simulated total spectrum; black curve, experimental.

pyrrole region with spin-lock times of 100 μs and 40 ms. Figure 5B shows the deconvoluted spectra with the C_α and C_β peaks identified. The signals of the C_α and C_β carbons are expected to split into two peaks each belonging to pyrrole (−NH ring) and pyrrolenine (=N ring) rings.[8] Crystal packing and intermolecular π-electron cloud effects are then considered for peak assignments.

Based on the literature,[8] $C_{\alpha,1}$ and $C_{\alpha,2}$ belonging to pyrrole ring (N−H) are expected to appear at a higher field (low chemical shift value) compared the $C_{\alpha,3}$ and $C_{\alpha,4}$ of the pyrrolenine (=N) ring. Again, based on distances, we expect to see four signals from the C_α carbons. $C_{\alpha,1}$ and $C_{\alpha,2}$ overlap to give a broad peak at 135.0 ppm. The two resonances at 150.5 and 149.3 ppm can be assigned to $C_{\alpha,3}$ and $C_{\alpha,4}$. This is also consistent with the fact that the three signals of C_α have the observed intensity ratio of 1:1:2. Similarly, we used the distance approach for the C_β with four expected resonances. The $C_{\beta,3}$ and $C_{\beta,4}$ belonging to pyrrolenine (=N) ring appear at a lower field compared to $C_{\beta,1}$ and $C_{\beta,2}$. $C_{\beta,3}$ and $C_{\beta,4}$ being less shielded from the neighboring π-electron cloud (compared to $C_{\beta,1}$ and $C_{\beta,2}$) should thus appear downfield. We assign $C_{\beta,3}$ at 143.1 ppm and $C_{\beta,4}$ at 140.8 ppm. $C_{\beta,1}$ and $C_{\beta,2}$ have very similar effects from the neighboring π-electron cloud, so we assign them as a single peak at 136.5 ppm. Thus, the high resolution attained using a single crystal has enabled us to detect the crystal packing and intermolecular π-electron cloud effects on the NMR spectra. Our results are consistent with only one dominant tautomeric form at room temperature in essential agreement with both Okazaki and Frydman.[7,8] In contrast, our peak assignments are in good agreement with the crystal structure.[18]

Peak Assignments for NiOEP. The metalated derivatives of OEP do not undergo N−H tautomerism, thus its NMR spectrum is simpler to analyze. The solid-state ^{13}C NMR spectrum of NiOEP was first reported by Okazaki and McDowell.[7] But likely due to the spectral overlap, their spectra did not correlate with the crystal structure;[19] however, they did speculate two peaks from all the carbons except the meso carbon. The ^{13}C peaks expected from the known crystal structure were not all resolved. In the present study, using a single crystal enabled us to observe the individual peaks. Figure 6 shows the comparison of powder and crystal NiOEP.

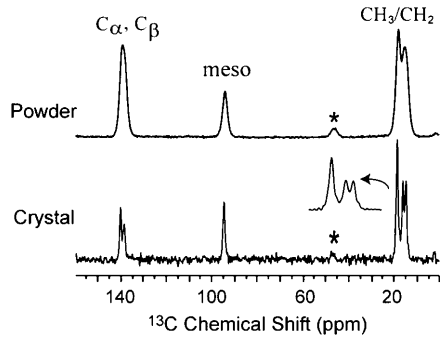

Figure 6. ^{13}C CP-MAS spectra of NiOEP from powder and a single crystal. The * represents a spinning sideband.

We observed a 2.2-fold resolution enhancement when we switched from powder to a crystal sample. The peak width at half-height decreased from 2.2 to 1.0 ppm. The relative area of the peak regions from C_α and C_β (combined), meso carbon, and CH_2−CH_3 (combined) were measured to be 3.0:1:5.6 and 2.0:1:5.0 from the powder and crystal spectra, respectively. Although such a small discrepancy could be attributed to the difference in the signal-to-noise ratio in the spectra, it is likely to be a result of the CP dynamics for a specific crystal orientation for the crystal sample, i.e., how the specific crystal was packed in the rotor, as opposed to that for all crystal orientations for the powder sample.

The spectra of crystal NiOEP consist of three peaks in the ethyl region with a singlet at 18.5 ppm and a doublet at 16.0 and 14.6 ppm. The singlet is of twice the intensity of each component of the doublet. Even so, it was still considered necessary to perform dipolar dephasing experiments to make a definitive assignment of these peaks.

Figure 7A shows the signals from the methylene and methyl carbons acquired with a dipolar dephasing duration of 2 μs while Figure 7B shows only the methyl region (18.5 ppm) acquired after a dipolar dephasing duration of 80 μs. Figure 7C is the subtraction spectra of Figure 7B from Figure 7A which results in the spectrum showing only the methylene region at 14.6 and 16.0 ppm This downfield shift of the CH_3 peak is unexpected and we explain this by the effect of intermolecular π-electron cloud due to the crystal packing arrangement in the

dx.doi.org/10.1021/jp302189r | J. Phys. Chem. B 2012, 116, 9215−9222

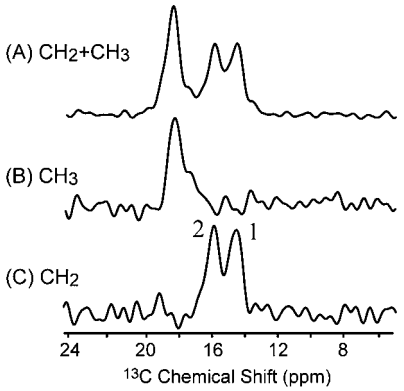

Figure 7. Peak assignment for the CH_2 and CH_3 signals from crystal NiOEP by dipolar dephasing using the dephasing time of (A) 2 μs and (B) 80 μs. (C) is the difference between (A) and (B). See text for detailed assignment.

unit cell.[19] From Table SI-1 (Supporting Information) it can be seen that the CH_2 carbons are more shielded by the neighboring π-electron cloud than CH_3 carbons. This makes them resonate at a high field. The two peaks from the CH_2 carbons can again be explained by the distance approach. It is seen that $CH_2(1)$ and $CH_2(2)$ are at different distances from the neighboring π aromatic electron cloud and henceforth they resonate at two different frequencies (Table SI-1, Supporting Information). The peak at 14.6 ppm is assigned to $CH_2(1)$ and that at 16.0 ppm to $CH_2(2)$. The CH_3 carbons should not be affected by the neighboring π-electron cloud owing to their much larger distance from the adjacent porphyrin moiety, resulting in a single resonance peak.

The signals from the C_α and C_β carbons were identified by $T_{1\rho}$ measurements. Figure 8 shows the C_α and C_β signals

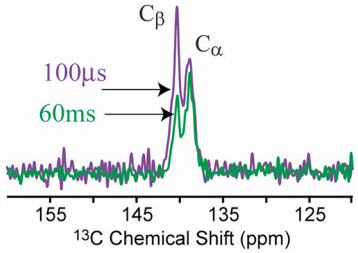

Figure 8. Peak assignment for the pyrrole region of crystal NiOEP by $T_{1\rho}$ measurement after spin lock times of 100 μs and 60 ms.

acquired after a spin-lock time of 100 μs and 60 ms. The rapidly dephasing peak at 140.3 ppm is assigned to the C_β and the peak at 138.7 ppm is from the C_α carbons. This high-field shift of the C_α carbons is because of the strong Ni–N bonding.[24] Based on the distance approach calculation (Table SI-1, Supporting Information), it was seen that both the $C_{\alpha,1,2}$ and $C_{\beta,1,2}$ carbons are at very similar distances from the neighboring π-electron clouds. Thus, these carbons are chemically and magnetically equivalent, giving rise to only one peak for each C_α and C_β. It is also noticed that carbons 3, 5, and 7 are magnetically equivalent to 1 and carbons 4, 6, and 8 are magnetically equivalent to 2 for all the C_α, C_β, CH_2, and CH_3 carbon atoms. Interestingly, Okazaki and McDowell observed only a single broad peak for the ethyl carbons, and another single peak for the pyrrole carbons. The failure to observe the nonequivalence of these carbons was attributed to an effective high (S_4) molecular site symmetry.[7] The presently obtained higher resolution and peak splitting shows that the S_4 symmetry argument is not valid; low resolution was the cause. Clear splitting is also observed in the methyl and methylene regions and pyrrole ring carbons. Our results are quite consistent with the crystal structure and without the need to invoke a S_4 symmetry. In fact, we are able to study separately the spin–lattice relaxation behavior of different types of methylene carbons (vide infra).

Peak Assignments for ZnOEP. In their pioneering experiments, Okazaki and McDowell attempted peak assignments for all the carbons in ZnOEP, but the spectral resolution attained in their study was insufficient to resolve the CH_2 peaks from CH_3 peaks. Also the crystal structure[20] was not available to them, prompting us to carry out detailed studies using single crystals.

ZnOEP crystals are long, thin, and needle shaped. The mass of just one single crystal was not sufficient to obtain a ^{13}C CP-MAS spectrum in reasonable time. So we used 10 crystals[14] of ZnOEP with their c axes parallel to the rotor axis. Solid-state ^{13}C CP-MAS spectra of ZnOEP in powder and crystal form are shown in Figure 9. Again, the crystals yielded about 150%

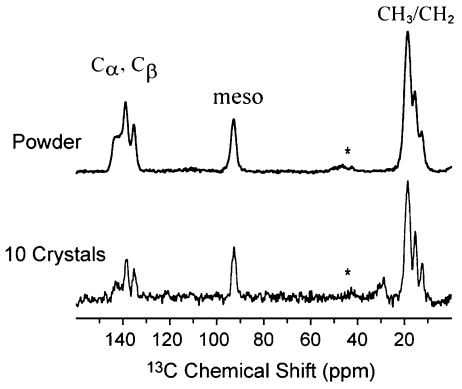

Figure 9. ^{13}C CP-MAS spectra of ZnOEP using powder and 10 single crystals, as indicated. The * is a broad sideband.

enhancement in resolution. The peak width at half-height decreased from 2.4 to 1.6 ppm. We conjecture that a big enough single crystal would lead to about 200% resolution enhancement. However, the sensitivity using ZnOEP crystals was seen to be insufficient to carry out dipolar dephasing and $T_{1\rho}$ experiments.

In order to identify the peaks from the methyl and methylene carbons, the dipolar dephasing measurements were made using the powdered sample. Figure 10A shows the spectra acquired

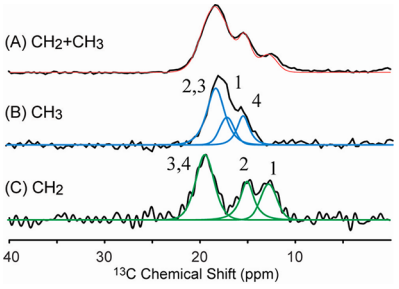

Figure 10. Spectra of ethyl region of ZnOEP obtained after a dephasing time of (A) 2 μs and (B) 80 μs. (C) Difference spectrum showing only the CH_2 component.

dx.doi.org/10.1021/jp302189r | J. Phys. Chem. B 2012, 116, 9215–9222

after a 2 μs delay with both methyl and methylene carbons signals, while Figure 10B shows the spectra acquired after 80 μs delay, where all the methylene carbons have dephased out and only signals from methyl carbons can be seen at 15.6, 17.2, and 18.4 ppm. Figure 10C shows the difference spectrum where only the signals from the CH_2 carbons can be seen at 12.8, 15.1, and 19.5 ppm.

The presence of the three peaks for CH_2 can be rationalized by using the distance approach from the crystal structure.[20] From the distance measurements (Table SI-1, Supporting Information), it can be seen that $CH_2(3)$ and $CH_2(4)$ are farthest from the neighboring π-electron cloud of the porphyrin moiety. They should be least shielded and hence most downfield shifted. $CH_2(3)$ and $CH_2(4)$ show strong overlapping and are hence assigned to the broad peak at 19.5 ppm. $CH_2(1)$ is slightly closer to the neighboring π-electron cloud compared to $CH_2(2)$. So, the former is less shielded and hence more upfield shifted compared to later. The resonance signal at 12.8 ppm is assigned to the $CH_2(1)$ and the signal at 15.1 ppm to $CH_2(2)$. The distance considerations show that the CH_2 carbons are located in three different environments and also explain the observed 2:1:1 intensity ratio.

The CH_3 resonance signals were also assigned in the same way. The signal at 15.6 ppm is assigned to $CH_3(4)$, signal from $CH_3(1)$ is at 17.2 ppm, and the signal at 18.4 ppm is from $CH_3(2, 3)$ (in magnetically similar environments). The observed intensity was in the ratio of 2:1:1. The CH_2 group is seen to be more shielded as compared to the CH_3 group due to its proximity to the porphyrin moiety and hence has a smaller isotropic chemical shift value but again they all overlap.

Similarly, $T_{1\rho}$ measurements enabled us to assign the C_α and C_β carbons. Figure 11A shows the spectra in the pyrrole region

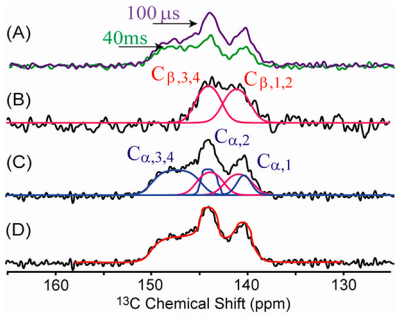

Figure 11. Peak assignment of C_α and C_β signals of ZnOEP using $T_{1\rho}$ measurements (A) after a spin-lock time of 100 μs and 40 ms. (B) Difference spectra of (A) showing only C_β carbons, (C) deconvolution of the spectrum after a spin lock time of 100 μs identifying both the of C_α and the C_β carbons, and (D) black curve, experimental; red curve, simulated total spectrum.

obtained for spin-lock times of 100 μs and 40 ms. Due to strong overlapping of the C_α and C_β signals, the rapidly decaying C_β signals could not be clearly identified. A difference spectrum was thus obtained. The difference of the spectra from the 100 μs and the 40 ms runs was adjusted in such a way that no signal from the C_α carbons could be seen but the signals from the C_β carbons were visible. The peaks were then deconvoluted (Figure 11B). Using the same intensity and the chemical shift positions of the C_β carbons as in Figure 11B, the C_α carbons were identified in Figure 11C—corresponding to a spin-lock time of 100 μs. Figure 11D shows the total simulated spectrum after identifying both C_α and C_β.

The splitting of the C_α and C_β carbon signals can be explained on the basis of the crystal packing effect and the distance approach model. The crystal structure[20] shows that the C_α and C_β carbons have different local environments. By looking at the distance values (Table SI-1, Supporting Information), $C_{\alpha,1}$ is at the maximum distance from the neighboring π-electron cloud and should appear most downfield. However, because of its spatial proximity to the core of the π-electron cloud (N atom), it becomes highly shielded and appears at the lowest shift of 135.5 ppm. Similarly, $C_{\alpha,2}$ appears next at 139.1 ppm. $C_{\alpha 3}$ and $C_{\alpha 4}$ are in magnetically similar environment (distance from neighboring π-electron cloud) and so appear together at a lower field of 142.4 ppm. This peak is quite broad, implying that the resonance signals of $C_{\alpha,3,4}$ are not exactly the same, but show a strong overlap. The splitting in the C_β peaks can also be rationalized in the same way: $C_{\beta,1,2}$ are closest to the neighboring π-electron cloud and so are more shielded. They are also spatially closer to the neighboring π-electron cloud (proximity to N). Thus, they are assigned at a lower shift value of 136.1 ppm and $C_{\beta,3,4}$ are assigned at 139.0 ppm.

The C_α, C_β peaks show a strong overlap because they are all at very similar distances to the neighboring π-electron cloud. Local electronic environment of carbon atoms of groups 5, 6, 7, and 8 were found to be similar to those of 1, 2, 3, and 4, respectively. All the chemical shifts are collated in Table 1.

It should be noted that all the powder MAS spectra reported here were obtained using a powder sample made by crushing several small single crystals. This justifies that the improved resolution on going from a powder to a single crystal is solely due to ABMS. To reconfirm this important point, we later duplicated the measurement for NiOEP comparing spectra from a powder by crushing several good single crystals, and a powder without recrystallization (used as purchased). The obtained spectra were essentially identical (shown in Figure SI-1 in Supporting Information).

Motional Dynamics of CH_2 and CH_3 Moieties in NiOEP. The success of the assignment of the individual peaks enabled us to probe the dynamics of the CH_2 and CH_3 carbons of the octaethyl moieties, via spin relaxation time, T_1 measurements. NiOEP was chosen for this preliminary feasibility study because of its large crystal size and good stability. T_1 was measured using the inversion recovery as outlined in the Experimental Section. Figure 12 shows the

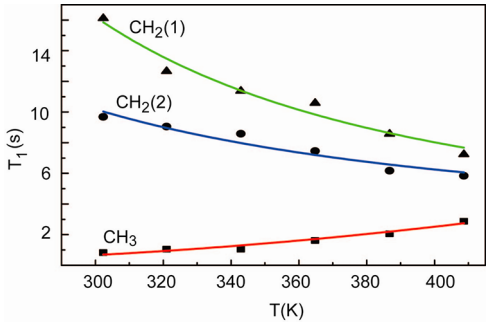

Figure 12. Temperature dependence of T_1 for the CH_3, $CH_2(1)$, $CH_2(2)$ carbons of single crystal NiOEP. Solid squares show the T_1 for the CH_3 carbons and the red line the BPP fit. Black circles represent T_1 for CH_2 (2) and the blue line its BPP fit. Black triangles show the T_1 for $CH_2(1)$ carbons, with the green line its BPP fit. The error bars are within the symbol sizes.

dx.doi.org/10.1021/jp302189r | J. Phys. Chem. B 2012, 116, 9215−9222

temperature dependence of T_1 for the methyl and two CH_2 carbons 1 and 2 from 300 to 400 K. It is seen that, for the CH_3 carbons, T_1 increases with temperature while for both the CH_2 carbons T_1 decreases albeit at slightly but significantly different rates, i.e., with different activation energies.

The temperature dependence of T_1 was analyzed using the Bloembergen, Purcell, and Pound (BPP)[25] model wherein T_1 is related to a correlation time, τ_c, which is the characteristic time between significant fluctuations in the local magnetic field experienced by a spin due to molecular motions or reorientations of a molecule. It is assumed that the temperature dependence of τ_c follows Arrhenius-like behavior:

$$\tau_c = \tau_0 \exp(E_a/RT) \quad (1)$$

$$\frac{1}{T_1} = C\left(\frac{\tau_c}{1 + (\varpi_H - \varpi_C)^2\tau_c^2} + \frac{3\tau_c}{1 + \varpi_C^2\tau_c^2} + \frac{6\tau_c}{1 + (\varpi_H + \varpi_C)^2\tau_c^2}\right) \quad (2)$$

The symbols have their standard meanings. The constant C and τ_c is given for a heteronuclear dipole−dipole interaction as[25−27]

$$C = \frac{1}{10}\left(\frac{\mu_0}{4\pi}\frac{\gamma_H\gamma_C\hbar}{r_{CH}^3}\right)^2 \quad (3)$$

where ω_C and ω_H are the resonance frequencies of ^{13}C and ^1H; r_{CH} is the average C−H bond distance and γ_C and γ_H are the gyromagnetic ratios of ^{13}C and ^1H, respectively. τ_0 and E_a were taken as fit parameters. The solid lines in Figure 12 show the fit to eqs 1, 2, and 3. The fitting parameters are summarized in Table SI-2 (Supporting Information). C was calculated from eq 3 using the C−H bond distance from the crystal structure.[19]

The τ_0 and E_a values (Table SI-2, Supporting Information) enabled us to calculate the correlation times, τ_c, for the ^{13}C CH_2 and CH_3 sites (Figure 13). τ_c was calculated using eq 1.

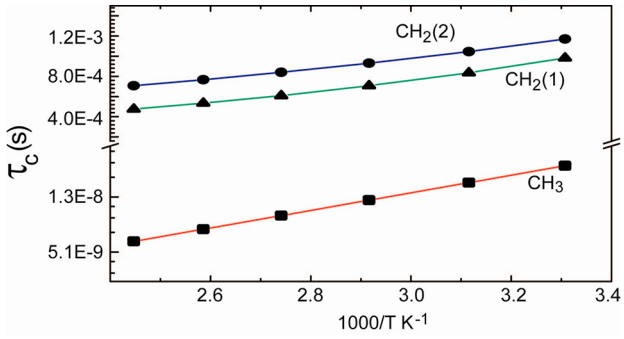

Figure 13. Temperature dependence of correlation time, τ_c, for the ethyl carbons in single crystal NiOEP.

The decrease of τ_c at higher temperature indicates that the bond motion becomes faster at higher temperatures. From the crystal structure it can be seen that the CH_2−CH_3 motion is sterically hindered, which also provides a rationale for the observed higher activation energy of CH_3 (13.2 kJ/mol) compared to that of CH_2.

It is also seen that the activation energy for $CH_2(1)$ is slightly higher than that for $CH_2(2)$. Again, this can be attributed to the closer proximity of the neighboring π-electron cloud to $CH_2(1)$.

4. CONCLUSIONS

We have documented that the standard high-resolution, CP-MAS, ^{13}CNMR spectra of powder octaethyl porphyrin and its Ni and Zn derivatives are broadened by a factor of 2 due to their anisotropic bulk magnetic susceptibility (ABMS). The utilization of single crystals in MAS measurements removed that broadening. The obtained resolution enhancement (~200%) enabled us to make much more definitive peak assignments. The assignment procedure utilized the so-called atomic distance approach as well the π-electron cloud effect on shielding and chemical shifts. For several peaks, the current assignments differ significantly from the literature.[7,8] For NiOEP, in contrast to earlier reports, the current study shows peak splittings that directly point to a breakdown of the S_4 symmetry, rendering the NMR conclusions consistent with the X-ray crystal structure. Moreover, for NiOEP, we were able to study the spin−lattice relaxation behavior of the $-CH_2$ and $-CH_3$ carbons of the ethyl chains, and thereby the molecular motion of these moieties. Such detailed studies are very difficult, if not impossible, with MAS using powders of these materials, because of strong peak overlapping, and thus difficulties due to spin diffusion. For the case of ZnOEP, earlier studies had attributed the lack of peak splitting to similarities of the crystal structures of OEP and ZnOEP. The present results show that it is actually due to essential broadening in the powder spectra, since the crystal structures of OEP and ZnOEP are similar ($P\bar{1}$). Our results show that peak splitting in the ethyl region for ZnOEP is less than 1 ppm different than OEP again, an indication of a similarity in their crystal structures, but the resolution of crystal method is good enough to resolve these closely spaced peaks. We thus envisage that the significantly higher resolution afforded by the use of a single crystal or highly oriented samples in MAS measurements should find wider applications in structural and dynamical studies than previously thought.

■ ASSOCIATED CONTENT

Supporting Information

Table SI-1, shortest distances (Å) of the observed carbon atom from the two closest atoms of the neighboring molecule as obtained from the crystal structures; Table SI-2, fitting parameters from BPP; and Figure SI-1, ^{13}C CP-MAS of single crystal, crushed crystals, and powder NiOEP obtained from a 600 MHz (^{1}H) spectrometer. This material is available free of charge via the Internet at http://pubs.acs.org.

■ AUTHOR INFORMATION

Corresponding Author

*E-mail: rfu@magnet.fsu.edu (R.F.); dalal@chem.fsu.edu (N.S.D.).

Notes

The authors declare no competing financial interest.

■ ACKNOWLEDGMENTS

We are grateful to Drs. Alan Marshall, Ryan Rogers, and Amy McKenna for their encouragement and valuable discussions. Much of the experimental work was carried out at the National High Magnetic Field Laboratory (NHMFL) supported by the NSF Cooperative agreement No. DMR-0654118 and the State of Florida. We are grateful to Dr. Ron Clark at Florida State University for his help with crystallography.

REFERENCES

(1) Dolphin, D. *The Porphyrins*; Academic Press: New York, 1977.
(2) Callot, H. J.; Ocampo, R. *The Porphyrin Handbook*; Academic Press: New York, 2000; Vol. *1*.
(3) (a) Filby Royston, H.; Van Berkel Gary, J. *Metal Complexes in Fossil Fuels*; American Chemical Society: Washington, DC, 1987; Vol. *344*, p 2; (b) Quirke, J. M. E. *Metal Complexes in Fossil Fuels*; American Chemical Society: Washington, DC, 1987; Vol. *344*, p 308.
(4) Storm, C. B.; Teklu, Y. *J. Am. Chem. Soc.* **1972**, *94*, 1745−1746.
(5) Abraham, R. J.; Hawkes, G. E.; Smith, K. M. *Tetrahedron Lett.* **1974**, 1483−1486.
(6) Abraham, R. J.; Hawkes, G. E.; Smith, K. M. *J. Chem. Soc., Perkin Trans. 2* **1974**, 627−634.
(7) Okazaki, M.; McDowell, C. A. *J. Am. Chem. Soc.* **1984**, *106*, 3185−3190.
(8) Frydman, L.; Olivieri, A. C.; Diaz, L. E.; Valasinas, A.; Frydman, B. *J. Am. Chem. Soc.* **1988**, *110*, 5651−5661.
(9) Pines, A.; Gibby, M. G.; Waugh, J. S. *J. Chem. Phys.* **1973**, *59*, 569−590.
(10) Levitt, M. H. *Spin Dynamics: Basics of Nuclear Magnetic Resonance*, 2nd ed.; Wiley and Sons Ltd.: New York, 2002.
(11) Lowe, I. J. *Phys. Rev. Lett.* **1959**, *2*, 285−287.
(12) Andrew, E. R.; Bradbury, A.; Eades, R. G. *Nature* **1959**, *183*, 1802−1803.
(13) Vanderhart, D. L.; Earl, W. L.; Garroway, A. N. *J. Magn. Reson.* **1981**, *44*, 361−401.
(14) (a) Klymachyov, A.; Dalal, N. *Solid State Nucl. Magn. Reson.* **1997**, *9*, 85−89. (b) Klymachyov, A. N.; Dalal, N. S. *Z. Phys. B Condens. Matter* **1997**, *104*, 651−656. (c) Dalal, N.; Klymachyov, A.; Bussmann-Holder, A. *Phys. Rev. Lett.* **1998**, *81*, 5924−5927.
(15) Vasa, S. K.; Janssen, H.; Van Eck, E. R. H.; Kentgens, A. P. M. *Phys. Chem. Chem. Phys.* **2011**, *13*, 104−106.
(16) Vasa, S. K.; van Eck, E. R. H.; Janssen, J. W. G.; Kentgens, A. P. M. *Phys. Chem. Chem. Phys.* **2010**, *12*, 4813−4820.
(17) Kunath-Fandrei, G. H.; Kelbauskas, L.; Döring, D.; Rager, H.; Jäger, C. *Phys. Chem. Miner.* **1998**, *26*, 55−62.
(18) Lauher, J. W.; Ibers, J. A. *J. Am. Chem. Soc.* **1973**, *95*, 5148−5152.
(19) Meyer, E. F. *Acta Crystallogr., Sect. B* **1972**, 2162.
(20) Ozarowski, A.; Lee, H. M.; Balch, A. L. *J. Am. Chem. Soc.* **2003**, *125*, 12606−12614.
(21) Bennett, A. E.; Rienstra, C. M.; Auger, M.; Lakshmi, K. V.; Griffin, R. G. *J. Chem. Phys.* **1995**, *103*, 6951−6958.
(22) Opella, S. J.; Frey, M. H. *J. Am. Chem. Soc.* **1979**, *101*, 5854−5856.
(23) Ye, C. H.; Fu, R. Q.; Hu, J. Z.; Hou, L.; Ding, S. W. *Magn. Reson. Chem.* **1993**, *31*, 699−704.
(24) Kawano, K.; Ozaki, Y.; Kyogoku, Y.; Ogoshi, H.; Sugimoto, H.; Yoshida, Z. I. *J. Chem. Soc., Perkin Trans. 2* **1978**, 1319−1325.
(25) Bloembergen, N.; Purcell, E. M.; Pound, R. V. *Phys. Rev.* **1948**, *73*, 679−712.
(26) Gunaydin-Sen, O.; Achey, R.; Dalal, N. S.; Stowe, A.; Autrey, T. *J. Phys. Chem. B* **2007**, *111*, 677−681.
(27) Mehring, M. *Principles of high-resolution NMR in solids*, 2nd ed. (revised and enlarged); Springer-Verlag: Berlin, 1983.